Aharonov-Casher phase in an atomic system

Karin Sangster and E. A. Hinds
Physics Department, Yale University, New Haven, Connecticut 06520

Stephen M. Barnett, Erling Riis, and A. G. Sinclair
Department of Physics and Applied Physics, University of Strathclyde, Glasgow G4 0NG, Scotland
(Received 22 September 1994)

We describe an experimental configuration suitable for observing the geometric phase of Aharonov and Casher in atomic systems. Using this we have been able to show experimentally that the Aharonov-Casher phase is both independent of velocity and proportional to an electric field and we have verified the predicted size of the effect with an accuracy of 2%.

PACS number(s): 03.65.Bz

I. INTRODUCTION

In 1984, Aharonov and Casher [1] considered a particle with magnetic dipole moment μ being taken on a closed path around a charged wire. They predicted that the wave function of the particle should acquire a phase shift

$$\Delta\Phi_{\mathrm{AC}}=\frac{1}{\hbar c^2}\oint \mu\times\mathbf{E}\cdot d\mathbf{r}\ , \tag{1}$$

where $\mathbf{E}$ is the electric field at the site of the dipole due to the wire. When the wire carries a constant charge per unit length Λ and when the component $\mu_\perp$ of μ along $\mathbf{E}\times d\mathbf{r}$ is constant around the loop, the accumulated phase $\Delta\Phi_{\mathrm{AC}}$ is equal to $\mu_\perp\Lambda/\varepsilon_0\hbar c^2$ independent of the path. This result is independent of the (constant) cross section of the wire, the path which encloses it, and the velocity of the particle. In this restricted sense, the Aharonov-Casher (AC) phase is a geometric one, analogous to the Aharonov-Bohm effect [2] in which a charged particle acquires a path-independent phase when taken around a tube of magnetic flux. In the Aharonov-Bohm case, there are no such restrictions because the flux enclosed by the path is uniquely defined and the charge has no additional degrees of freedom analogous to the orientation of the magnetic moment. It is a characteristic feature of both these effects that the phase shift is independent of the velocity of the particle [3] and that there is no force on the particle [4].

The AC effect was first tested in a neutron interferometer [5], where a beam of neutrons was coherently split, as illustrated in Fig. 1(a), allowed to encircle a line charge, and then recombined to give an interference pattern. The measured phase shift was 2.11 ± 0.34 mrad, compared with the predicted value of 1.52 mrad. Although the observed phase was nearly two standard deviations above the theoretical value, the experiment did seem to confirm the existence of the effect. However, there was no experimental verification of the two most notable features: velocity independence and proportionality to an electric field. Subsequently, there were suggestions for observing the AC effect in similar interferometers using atoms instead of neutrons [6], but the first results using atoms and the first tests of the velocity and field dependence were obtained by a different technique and were recently described in a preliminary publication from our laboratory [7]. This paper gives a fuller account of that work together with substantial additional results which lead to a more stringent test of the theory.

The scheme shown in Fig. 1(a) involves two coherent beams with the *same* magnetic moment traveling on *different* paths around a charged wire. The beam on path a acquires an AC phase shift

$$\Phi_a=\frac{1}{\hbar c^2}\int \mu\times\mathbf{E}(\mathbf{r}_a)\cdot d\mathbf{r}_a\ . \tag{2}$$

A similar expression applies to path b and the net accumulated phase difference $\Delta\Phi=\Phi_a-\Phi_b$ is given by Eq. (1). It is not necessary for the paths to enclose a line of charge in order to observe the AC effect; indeed, Casella has noted [8] that Φ_a and Φ_b can be made different by a simple arrangement of capacitor plates, which ensures that the electric fields have opposite polarity on the two paths. In Ref. [7] we pointed out a third possible configuration, shown in Fig. 1(b), where the two coherent

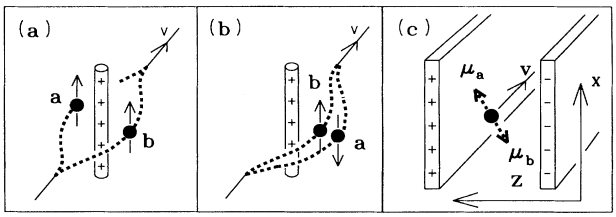

FIG. 1. Experimental configurations for observing the Aharonov-Casher effect. (a) Geometry of the original measurement using a neutron interferometer, in which the two interfering states encircle a charge and have the same magnetic moments. (b) Geometry described here. Particles travel in a uniform electric field in a coherent superposition of states a and b with different magnetic moments μ_a and μ_b. The two states are oppositely shifted by the Aharonov-Casher phase as they travel through the field.

beams have *different* magnetic moments (μ_a and μ_b) and are not spatially separated; they pass through the *same* electric field. In this arrangement the AC phase shift between the two arms of the interferometer is given by

$$\Delta\Phi_{\rm AC}=\frac{1}{\hbar c^2}\int(\mu_a-\mu_b)\times\mathbf{E}\cdot d\mathbf{r}\ . \tag{3}$$

For simplicity we assume, as shown in Fig. 1(c), that the beam travels a distance L along the y axis and that $\mathbf{E}$ lies in the z direction; then the x component of the magnetic moment is the only relevant one and

$$\Delta\Phi_{\rm AC}=\frac{1}{\hbar c^2}([\mu_x]_a-[\mu_x]_b)EL\ . \tag{4}$$

The loop corresponding to the two paths in the interferometer does not now enclose any line charge and therefore appears different from the situation considered by Aharonov and Casher. We have taken advantage of the fact that μ in Eq. (1) need not be fixed with respect to $\mathbf{E}\times d\mathbf{r}$ in order to obtain a nonvanishing path integral. It is worthwhile to note, however, that path a of Fig. 1(b) can be continuously deformed at constant $\Delta\Phi_{\rm AC}$ to recover the geometry of Fig. 1(a) by passing over the end of the line charge or, if it is infinitely long, through an infinitesimal cut in the line. This is possible because the AC phase is not geometric, except when the direction of μ is constrained, as discussed in the opening paragraph.

It is by no means necessary to use neutrons; any neutral particle with a magnetic moment should exhibit the AC effect; all that is required is a convenient way of preparing the magnetic moment in a coherent superposition of two states with different values of μ_x and detecting the accumulated AC phase difference. We have chosen to use Ramsey's method of separated oscillatory fields [9], in which the first field prepares a coherent superposition of two spin states ($[\mu_x]_a$ and $[\mu_x]_b$) and the second probes the phase that has evolved between them. Thus the experiment involves magnetic resonance in the presence of an electric field. When the electric field polarity is reversed, the sign of the AC phase changes and this appears as a phase shift of the Ramsey resonance line.

The AC phase shift has an interesting interpretation when viewed from the rest frame of the atom. Here there is no displacement ($d\mathbf{r}=0$), but there is a motional magnetic field arising from the laboratory frame electric field. From this point of view then, the AC phase shift is the integral over time of the motional Zeeman energy:

$$\frac{1}{\hbar}\int(\boldsymbol{\mu}\cdot\mathbf{B}dt)_{\rm atom}=\frac{1}{\hbar c^2}\int(\boldsymbol{\mu}\times\mathbf{E}\cdot d\mathbf{r})_{\rm lab}=\Phi_{\rm AC}\ , \tag{5}$$

where the subscripts atom and lab refer to the atom and laboratory frames of reference, respectively. The magnitude of the shift is, of course, the same in any frame of reference. The motional Zeeman effect has been recognized as a source of systematic error [10] in atomic beam experiments [11,12], which test time-reversal symmetry by looking for a permanent atomic electric-dipole moment (EDM). However, this connection with the AC phase has been overlooked until now and the effect has therefore escaped thorough experimental investigation, although some early data ascribed to the motional Zeeman effect do suggest linearity in the electric field [10]. In EDM beam experiments, the effect is usually suppressed as much as possible with the help of a magnetic bias field parallel to the strong applied electric field. This forces the magnetic moment to be quantized parallel to the electric field, ensuring that $\boldsymbol{\mu}\times\mathbf{E}=0$. The bias field can either be a carefully aligned external field [12] or, in the case of a polar diatomic molecule [11], it can be the internal magnetic field of the molecule.

We observe the AC phase using the fluorine nuclei in a thallium fluoride (TlF) molecular beam in a strong (10–30 kV/cm) external electric field $\mathbf{E}$. The molecules are in the electronic and vibrational ground states $^1\Sigma^+$, $v=0$, and in the first excited rotational state $J=1$. The rotational states are strongly mixed by the applied electric field, so J is not a good quantum number, but it serves adequately to identify which rotational state we use. Within the $J=1$ manifold there are 12 hyperfine sublevels corresponding to the magnetic quantum numbers of the rotation ($m_J=0,\pm1$), Tl nuclear spin ($m_{\rm Tl}=\pm\frac{1}{2}$), and F nuclear spin ($m_{\rm F}=\pm\frac{1}{2}$). In a strong electric field, these separate into four $m_J=0$ and eight $m_J=\pm1$ states, the latter being the relevant ones for our experiment. Figure 2 shows the energies of the eight states and labels them 1 through 8. We also show the transitions 2-3 and 6-7 that were studied in this experiment, which correspond closely to simple flips of the fluorine nuclear spin.

Using techniques that are described more fully below and elsewhere [11], we first prepare the molecules in the initial state a ($a=2$ or 6). The beam then passes through the first of two Ramsey loops [9] in which an rf magnetic field near-resonantly excites a coherent superposition of the states a and b ($b=3$ or 7) with roughly equal amplitudes. This loop is effectively the beam splitter of our interferometer, providing the required coherent superposition of magnetic moments μ_a and μ_b. The molecules travel in this state for a distance L before reaching the second rf loop which plays the role of the recombining beam splitter. The rest of the apparatus then determines what fraction P of the molecules made the transition from a to b. Close to resonance, the Ramsey fringe pat-

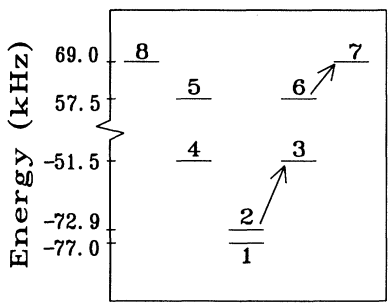

FIG. 2. Energy levels for the eight $|J=1,|m_J|=1\rangle$ states of thallium fluoride in an electric field of 20.0 kV/cm. The two transitions marked (2-3 and 6-7) correspond closely to fluorine spin flips and were used for the experiments described here.

tern has the usual form [9]

$$P=\tfrac{1}{2}\left[1+\cos\left[(\omega-\omega_0)\frac{L}{v}+\delta+\Delta\Phi\right]\right], \tag{6}$$

where ω is the rf frequency, ω_0 is the resonance frequency, v is the beam velocity, δ is the phase difference between the two rf fields, and $\Delta\Phi$ is any additional phase shift between the two states a and b in the interferometer, such as the AC phase.

Since the molecule in external electric field is cylindrically symmetric around the field direction z, the expectation value of the transverse magnetic moment μ_x is zero in any of these states. It follows from Eq. (4) that the AC effect is completely suppressed. While this is a great advantage in the search for an EDM, where the AC effect is a potential source of systematic error, it is obviously an obstacle to be overcome in the present context. In order to study the AC phase, we must rotate the magnetic symmetry axis so that the magnetic moment of the molecule can have a nonzero projection μ_x. This is done by applying a uniform magnetic field **B** along the x axis, as shown in Fig. 3.

To summarize, the experiment involves a radio-frequency transition between two hyperfine sublevels a and b of the TlF molecule, which are separated in energy by $\hbar\omega_0$. A magnetic field B_x induces transverse magnetic moments $[\mu_x]_a$ and $[\mu_x]_b$ and a strong electric field E_z induces an AC phase shift between the two levels (in addition to the usual $\omega_0 t$ due to the energy difference between the levels). When either applied field is reversed, the AC phase changes sign, allowing us, with the help of Eq. (6), to deduce $\Delta\Phi$ from the measured changes in the transition probability P. This experimental phase shift is compared with a theoretical prediction (based on Eq. (4) together with the calculated value of $[\mu_x]_a-[\mu_x]_b$) in order to test the validity of the theory.

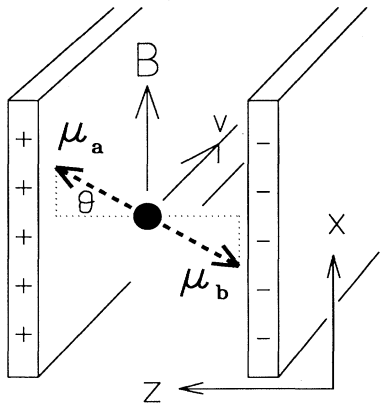

FIG. 3. Field configuration for this experiment. Thallium fluoride molecules prepared in a coherent superposition of opposite spin states travel through an electric field. The natural alignment of the spins is along the electric field (z axis), so a magnetic field B_x is used to give them a perpendicular component.

II. RELATIVISTIC ANALYSIS OF THE AC EFFECT

We have noted that the AC phase shift has an appealing interpretation, when viewed in the atomic frame, as a Zeeman shift induced by the motional magnetic field. This appeal to relativity is interesting as the molecule has a velocity very much less than the speed of light and the AC phase shift is predicted to be a velocity-independent effect. Furthermore, the original derivation of the AC phase was based on the nonrelativistic Schrödinger equation. It is worthwhile to see how the AC shift arises within a relativistic analysis and to ask whether its predicted velocity independence still holds at velocities within the relativistic regime. Relativistic analyses based on the Dirac equation for a magnetic dipole have been given by others (including Aharonov and Casher themselves [1] and Hagen [2]); however, the geometry of our experiment, with constant electric and magnetic field, permits a particularly simple treatment.

Our starting point is the Dirac Hamiltonian for a free, spin-$\frac{1}{2}$ particle with rest mass m, which can be written as a 4×4 matrix composed of a 2×2 blocks

$$H_0=\begin{bmatrix}1mc^2 & \sigma\cdot\mathbf{p}c\\ \sigma\cdot\mathbf{p}c & -1mc^2\end{bmatrix}, \tag{7}$$

where **1** is the unit matrix, the components of σ are the Pauli matrices, **p** is the linear momentum, and c is the speed of light. If the particle is uncharged, but has magnetic dipole moment μ, then the interaction with external (laboratory frame) electric and magnetic fields **E** and **B** can be expressed by the addition to H_0 of the interaction term [13]

$$V=\mu\begin{bmatrix}-\sigma\cdot\mathbf{B} & i\sigma\cdot\mathbf{E}/c\\ -i\sigma\cdot\mathbf{E}/c & \sigma\cdot\mathbf{B}\end{bmatrix}. \tag{8}$$

The quantities μB and $\mu E/c$ are exceedingly small in comparison with mc^2, even if m is as light as the electron mass and μ is as large as the Bohr magneton. This allows us to treat V as a small perturbation to H_0 in any realistic situation and in particular in our experiment where the mass and magnetic dipole moment are those of the fluorine nucleus.

H_0 has two eigenvalues $\pm\mathcal{E}_0$, given by

$$\mathcal{E}_0=\pm c\sqrt{m^2c^2+p^2}, \tag{9}$$

and for each eigenvalue there are two degenerate eigenstates corresponding to spin up and spin down. The two positive-energy eigenfunctions can be written as a 4×2 matrix in the form

$$M=\frac{1}{\sqrt{2\mathcal{E}_0(\mathcal{E}_0+mc^2)}}\begin{bmatrix}1(\mathcal{E}_0+mc^2)\\ \sigma\cdot\mathbf{p}c\end{bmatrix}. \tag{10}$$

In the nonrelativistic regime, with $mc^2\gg pc$, these reduce to two-component eigenstates of the Pauli operator σ_z; however, we will work with the fully relativistic free-particle eigenstates of Eq. (10) as we wish to examine the relativistic properties of the AC phase shift. We will

use degenerate perturbation theory to calculate the energy-level splitting of these two states which results from the applied fields. In our experiment, the fields are uniform, so the matrix elements of the perturbation V are diagonal in $\mathbf{p}$. This means that the new states are also eigenstates of momentum. Hence the shifts of the positive-energy states with momentum $\mathbf{p}$ are given by the eigenvalues of the 2×2 matrix

$$\Delta = M^\dagger V M \ . \tag{11}$$

After some algebra, and after using the identity

$$\mathbf{a}\cdot\boldsymbol{\sigma}\mathbf{b}\cdot\boldsymbol{\sigma} = \mathbf{a}\cdot\mathbf{b} + i\mathbf{a}\times\mathbf{b}\cdot\boldsymbol{\sigma} \ , \tag{12}$$

one finds that Δ can be written as

$$\Delta = \mu\left[-\boldsymbol{\sigma}\cdot\mathbf{B} + \frac{\mathbf{p}\times\mathbf{E}\cdot\boldsymbol{\sigma}}{\mathscr{E}_0} + \frac{c^2\mathbf{B}\cdot\mathbf{p}\boldsymbol{\sigma}\cdot\mathbf{p}}{\mathscr{E}_0(\mathscr{E}_0+mc^2)}\right] . \tag{13}$$

Diagonalizing this 2×2 matrix leads to the eigenvalues $\pm\delta\mathscr{E}$, where

$$(\delta\mathscr{E})^2 = \mu^2\left[\left[\mathbf{B} - \frac{\mathbf{p}\times\mathbf{E}}{\mathscr{E}_0}\right]^2 - \frac{c^2(\mathbf{B}\cdot\mathbf{p})^2}{\mathscr{E}_0^2}\right] . \tag{14}$$

The easiest way to see this is to notice that Δ^2 is diagonal, with eigenvalues given by $(\delta\mathscr{E})^2$ above.

Our molecular beam is not, of course, in a pure state of momentum $\mathbf{p}$ since thermal equilibrium in the oven produces a broad statistical mixture of momenta satisfying the Maxwell-Boltzman distribution. More precisely, we have a mixture of states, each with a narrow coherent momentum spread $\Delta\mathbf{p}$, comparable with $\hbar/\Delta x$, where Δx is a characteristic dimension of the source. Hence the quantity $\mathbf{p}/\mathscr{E}_0$ in Eq. (14) should be replaced by the appropriate expectation value for a wave packet of width $\Delta\mathbf{p}$ formed by superposing positive-energy eigenfunctions of H_0+V. These in turn can be expressed in terms of the positive-energy eigenfunctions of H_0, the free-space Hamiltonian, because within our degenerate perturbation theory, V does not couple the positive- and negative- energy eigenstates of H_0. For any such positive-energy wave packet, the expectation value of $\mathbf{p}/\mathscr{E}_0$ is related [14] to the group velocity $\mathbf{v}$:

$$\left\langle\frac{\mathbf{p}}{\mathscr{E}_0}\right\rangle = \frac{\mathbf{v}}{c^2} \ . \tag{15}$$

The spread $\Delta\mathbf{p}$ of the wave packet is sufficiently small that $\langle\mathbf{p}/\mathscr{E}_0\rangle^2 = \langle(\mathbf{p}/\mathscr{E}_0)^2\rangle$ to an excellent approximation. Hence Eq. (14) can be rewritten as

$$(\delta\mathscr{E})^2 = \mu^2\left[\left[\mathbf{B} - \frac{\mathbf{v}\times\mathbf{E}}{c^2}\right]^2 - \frac{(\mathbf{B}\cdot\mathbf{v})^2}{c^2}\right] . \tag{16}$$

The change in the positive-energy eigenvalues $\pm\delta\mathscr{E}$, given by this equation, is correct to *all orders* in v/c. Corrections to $\delta\mathscr{E}$ of higher order in μ are smaller than this by factors $\mu B/\mathscr{E}_0$ or $\mu E/\mathscr{E}_0 c$ and are therefore negligible.

The phase shift $\Delta\Phi$ accumulated between the states after a time t is

$$\Delta\Phi = 2\delta\mathscr{E}t/\hbar = \frac{2\mu}{\hbar}\left[\gamma^2\left[\mathbf{B}_\perp - \frac{\mathbf{v}\times\mathbf{E}}{c^2}\right]^2 + (\mathbf{B}_\parallel)^2\right]^{1/2}\frac{t}{\gamma} \ , \tag{17}$$

where we have chosen to break up $\mathbf{B}$ into components parallel ($\mathbf{B}_\parallel$) and perpendicular ($\mathbf{B}_\perp$) to $\mathbf{v}$. The full phase-shift relevant in our experiment is obtained by averaging Eq. (17) over the thermal velocity distribution. The part of this phase shift associated with the electric field is the Aharonov-Casher phase. This is clearly independent of the velocity of the molecules because the distance traveled (in the laboratory frame) $L=vt$ is the same for all the molecules. As we have carried out a fully relativistic analysis, without restricting the velocity, we conclude that the Aharonov-Casher phase shift is fully independent of velocity.

A particular simple interpretation appears if we notice that the two terms in parentheses are the perpendicular and parallel components of the magnetic field $\mathbf{B}'$ viewed from the rest frame of the molecule. Similarly, the elapsed time in that frame of reference is $t'=t/\gamma$, while the phase shift remains invariant; $\Delta\Phi'$ is the same as $\Delta\Phi$. With these substitutions, Eq. (17) becomes

$$\Delta\Phi' = \frac{2\mu}{\hbar}B't' \tag{18}$$

and we see that in the rest frame of the particle, the full interaction (to all orders in v/c) gives rise to nothing more than the Zeeman shift. The expression for $\Delta\Phi$ in terms of the laboratory fields is simply that required by special relativity.

One of the remarkable features of the Aharonov-Casher phase shift is that it arises even though there is no force acting on the particle to accelerate or decelerate it [4]. It shares this features with the more familiar Aharonov-Bohm effect [2]. There has been some controversy on this point [15], so it is worthwhile showing that the molecules in our experiment do not experience any force. Equation (15) shows that the group velocity is proportional to the average, over a positive-energy wave packet, of the momentum divided by the energy. Hence the acceleration is

$$\mathbf{a} = \frac{ic^2}{\hbar}\left\langle\left[H, \frac{\mathbf{p}}{\mathscr{E}_0}\right]\right\rangle , \tag{19}$$

which is clearly zero as the Hamiltonian $H=H_0+V$ commutes with the momentum. This result seems quite natural since our fields do not vary in space (or time) and we would not expect a dipole to be accelerated by a uniform field.

III. THEORY OF THE AC EFFECT IN TlF

Equation (4) shows that in order to calculate the expected AC phase shift of a transition between levels a and b in TlF, we need to know the difference $[\mu_x]_a - [\mu_x]_b$ between the magnetic moments induced in the states a and b by the transverse magnetic field B_x (~ 1 G). Before proceeding to a detailed numerical computation of this,

we will develop the following simple analytical model which gives some useful physical insight into the problem.

We are interested in the case when the external electric field produces very strong mixing of the rotational levels, which means that the rotational angular momentum is coupled much more strongly to the electric field axis z than to any of the other angular momenta. In this high-field regime, the two transitions we have studied (a-b = 2-3 or 6-7) are quite well described as fluorine nuclear spin flips and the a-b transition frequency, which we call ω_0, indicates that there is a magnetic field B_0 of strength $\hbar\omega/2\mu_F$ at the site of the fluorine nucleus due to the various hyperfine interactions, as shown schematically in Fig. 4. This field is directed on average along the symmetry axis z, defined by the strong external electric field. When the transverse field B_x is applied, the magnitude of the net magnetic field increases to $\sqrt{B_0^2+B_x^2}$ and the fluorine nuclear spin flip frequency is given by

$$\omega^2=\omega_0^2+(2\mu_F B_x/\hbar)^2 , \tag{20}$$

where μ_F is the nuclear magnetic moment of fluorine and [9]

$$2\mu_F/h=4.007\,26(8)\ \text{kHz/G} . \tag{21}$$

The difference between the induced transverse magnetic moments of the spin-up and spin-down states is given by the derivative of the energy difference, $\hbar\partial\omega/\partial B_x$:

$$[\mu_x]_a-[\mu_x]_b=2\mu_F\sqrt{1-(\omega_0/\omega)^2} , \tag{22}$$

which is nothing more than $2\mu_F\sin\theta$ (see Fig. 4).

This simple model is essentially a two-level picture. In fact, the presence of other levels allows the Tl nucleus (as well as the fluorine) to be polarized by B_x, thereby causing B_0 to change with B_x. Also, to the extent that the induced thallium polarization is different for levels a and b, it contributes directly to the differential transverse magnetic moment. Nevertheless, we find that this model provides an excellent approximation and that these omissions can be corrected with high accuracy if we simply replace the bare fluorine moment μ_F in Eqs. (11) and (13) by a suitably "shielded" moment μ'.

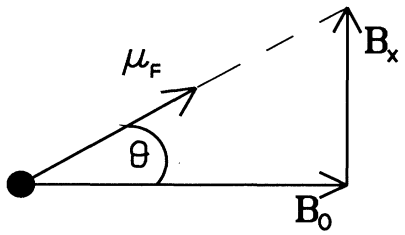

FIG. 4. Simple model of the transverse magnetization induced by B_x. When a transverse magnetic field B_x is added to the internal field B_0 due to hyperfine interactions, the net field is rotated by an angle θ. Hence the fluorine nuclear spin acquires a component $\mu\sin\theta$ along the x direction.

For our detailed theoretical prediction of the AC effect in TlF, we treated the molecule as a rigid rotor with the effective Hamiltonian [16]

$$H=hB_0\mathbf{J}^2-\mu_{el}\cdot\mathbf{E}+H_Z+H_{SR}+H_{SS} , \tag{23}$$

in which the first two terms are the rotational energy and the Stark interaction, respectively. The last three are the Zeeman, spin-rotation, and spin-spin interactions

$$H_Z=-\frac{\mu_J}{J}(\mathbf{J}\cdot\mathbf{B})-\frac{\mu_{Tl}}{I_{Tl}}(\mathbf{I}_{Tl}\cdot\mathbf{B})-\frac{\mu_F}{I_F}(\mathbf{I}_F\cdot\mathbf{B}) , \tag{24}$$

$$H_{SR}=c_1(\mathbf{I}_{Tl}\cdot\mathbf{J})+c_2(\mathbf{I}_F\cdot\mathbf{J}) , \tag{25}$$

$$H_{SS}=5c_3\left[\frac{3(\mathbf{I}_{Tl}\cdot\mathbf{J})(\mathbf{I}_F\cdot\mathbf{J})+3(\mathbf{I}_F\cdot\mathbf{J})(\mathbf{I}_{Tl}\cdot\mathbf{J})-2(\mathbf{I}_{Tl}\cdot\mathbf{I}_F)\mathbf{J}^2}{(2J+3)(2J-1)}\right]+c_4(\mathbf{I}_{Tl}\cdot\mathbf{I}_F) . \tag{26}$$

The values of the constants [9,16,17] are given in Table I. The frequencies of the a-b transitions in external fields E_z and B_x were computed by diagonalizing this Hamiltonian using a basis set that included rotational states up to $J=7$ (higher rotational states did not change the result). This detailed calculation of the eigenvalues showed that the frequencies of transitions 2-3 and 6-7 are indeed well described by an equation having the form of Eq. (20), but with a shielded moment μ' replacing μ_F. Specifically we found that

$$\omega^2=\omega_0^2+(2\mu' B_x/\hbar)^2 , \tag{27}$$

with μ' being constant to better than 0.2% when the fields B_x and E_z are varied anywhere in the ranges 0.3–2.0 G and 10–30 kV/cm, respectively. The shielded

TABLE I. The relevant interaction constants for ^{205}TlF in the electronic and vibrational ground state.

B_0/h	6 667 355.0(3) kHz[a]
μ_{el}/h	2128.5(4) kHz/(V/cm)[b]
μ_J/h	±0.038(15) kHz/G[b]
$\mu_{^{205}Tl}/h$	1.2403(3) kHz/G[c]
μ_F/h	2.003 41(15) kHz/G[c]
c_1/h	126.03(12) kHz[d]
c_2/h	17.89(15) kHz[d]
c_3/h	0.70(3) kHz[d]
c_4/h	−13.30(72) kHz[d]

[a]From the Dunham constants given in Table 2 of Ref. [16].
[b]Reference [17].
[c]Reference [9].
[d]Reference [16].

moments calculated in this way are given by

$$2\mu'_{2\text{-}3}/h = 3.95(2)\ \text{kHz/G}\ , \tag{28}$$

$$2\mu'_{6\text{-}7}/h = 3.86(2)\ \text{kHz/G}\ . \tag{29}$$

The intervals predicted by the Hamiltonian in Eq. (23) agree well with the hyperfine transition frequencies we observe in our own apparatus in a low field. However, in a strong external electric field, we find that the transition frequencies do not coincide exactly with the theoretical predictions. For example, in a field of 20 kV/cm and zero magnetic field, the calculated positions of the 6-7 and 2-3 transitions are 11.45 and 21.35 kHz, respectively, whereas the measured frequencies are 11.03 and 22.17 kHz. We believe that this is due to a modification of the hyperfine constants resulting from admixed excited electronic states, that is, the hyperfine constants change when the molecule is stretched by the electric field. The uncertainties given in Eqs. (28) and (29) are due to our corresponding uncertainty about the correct values of the hyperfine constants in a strong electric field. Fortunately, however, this Stark shift of the hyperfine constants leads to uncertainties in $\mu'_{2\text{-}3}$ and $\mu'_{6\text{-}7}$ that are less than 1%.

From the derivative of Eq. (27), we conclude that

$$([\mu_x]_3-[\mu_x]_2)/h = 3.95(2)\sqrt{1-(\omega_0/\omega)^2}\ \text{kHz/G} \tag{30}$$

and

$$([\mu_x]_7-[\mu_x]_6)/h = 3.86(2)\sqrt{1-(\omega_0/\omega)^2}\ \text{kHz/G}\ . \tag{31}$$

A comparison of these results with Eqs. (21) and (22) shows that the net effect of the other levels in the molecule is to reduce the μ_F of the two-level approximation by a few percent. Our predictions for the Aharonov-Casher phase shift are obtained by substitution of Eqs. (30) and (31) into Eq. (4).

IV. APPARATUS

A. Overview of experiment

A schematic of our TlF molecular-beam machine is shown in Fig. 5. The beam is produced by a supersonic jet source of TlF which increases our signal-to-noise ratio compared with an effusive beam by increasing the fraction of molecules in the lower rotational and vibrational states. After emerging from the source, molecules in the $|J=1, m_J=0\rangle$ rotational state are focused by an electrostatic quadrupole lens. These molecules are in four magnetic substates according to the orientation of the two spin-$\frac{1}{2}$ nuclei. They subsequently enter a region of constant, parallel magnetic and electric fields, labeled as the polarizer in Fig. 5, where an rf transition is driven from one of the four focused substates to one of the eight magnetic substates of the $|J=1, m_J=\pm 1\rangle$ manifold (see Fig. 2). Since the molecules are prepared in a single magnetic sublevel, the fluorine nucleus is now polarized.

The molecules continue on to the main interferometer region, where we apply a large electric field ($E_z=5-30$ kV/cm) in the z direction and a magnetic field ($B_x \sim 1$ G) in the x direction. Both fields are transverse to the molecular beam as shown in Fig. 3. As we remark in the Introduction, Ramsey's method of separated oscillating fields [9] provides the interferometer for our experiment. The first NMR loop generates an rf magnetic field in the y direction, which coherently splits the beam between two states of opposite fluorine nuclear polarization. These are allowed to evolve in the electric and magnetic fields for a distance L (~ 2 m), before being recombined by the second loop.

Finally, the molecules are analyzed by a second polarizer–quadrupole-lens combination (Fig. 5). Those in which the fluorine nuclear spin has not flipped are returned by the analyzer to their original state in the $|J=1, m_J=0\rangle$ manifold and are then focused by the quadrupoles onto a hot wire detector (oxygenated tungsten). By contrast, molecules whose fluorine nuclei have flipped in the Ramsey resonance region are not resonant with the rf field in the analyzer and cannot make a transition back to the $|J=1, m_J=0\rangle$ manifold. As a result, they are defocused by the second quadrupole and the Ramsey resonance appears as a decrease of the detected beam intensity.

Those parts of the apparatus which are particularly important to the Aharonov-Casher experiment are discussed in the following sections. A more complete discussion of the general operation of this TlF beam machine is given in Ref. [11].

B. Quadrupoles

In a strong electric field this polar molecule is well described as a rigid rotor with electric-dipole moment μ_{el}

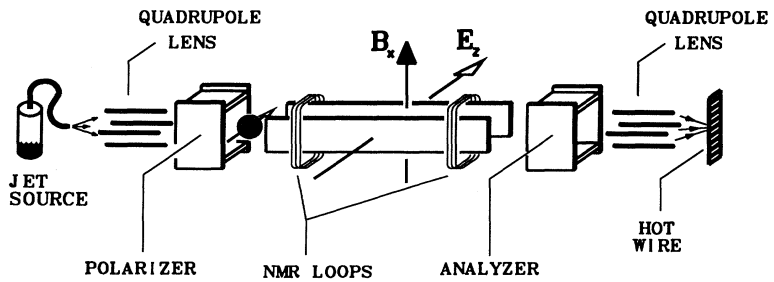

FIG. 5. Schematic view of the experiment. TlF molecules in rotational state $|J=1, m_J=0\rangle$ are focused by the electric quadrupole lens and make an rf transition in the polarizer to a single magnetic hyperfine sublevel of rotational state $|J=1, |m_J|=1\rangle$. Separated NMR loops drive a spin flip of the F nucleus. If the nucleus does not flip, the analyzer drives the rf transition back to the original $|J=1, m_J=0\rangle$ state, which is focused onto the detector. If the nucleus does flip, the molecules remain in rotational state $|J=1, |m_J|=1\rangle$ and are defocused.

[18] and (neglecting the hyperfine structure) the TlF Hamiltonian can be approximated by the first two terms in Eq. (23). The Stark interaction splits the rigid rotor levels into sublevels of different $|m_J|$ as we show for the rotational states $J=0,1,2$ in Fig. 6. As long as the electric field remains below the turnover point, the states having $|J=1,m_J=0\rangle$ are low-field seekers and are pushed toward the center (focused) in a quadrupole field, whereas the $|J=1,m_J=\pm 1\rangle$ states are defocused.

Each electrostatic quadrupole lens consists of four aluminum rods 60 cm long, having a semicircular cross section of radius 1.75 cm. The diameter of the inscribed circle of the assembled quadrupoles is 1.16 cm. We apply a potential difference across the rods in the range 12–30 kV, creating a quadrupole electric field whose magnitude is zero at the center and increases linearly to ~10–25 kV/cm at the edge. Normally, the same potential difference is applied across both quadrupoles to make a pair of lenses with equal power. Since the focal length also depends strongly on the velocity of the molecule, only a relatively narrow slice of the velocity distribution in the molecular beam ($\Delta v/v \sim 25\%$) is focused onto the detector at one time. The mean velocity of this slice can be varied in order to test the velocity independence of the AC phase simply by changing the potential on the quadrupoles. We note in passing that some slow molecules in the $J=2$ (and higher) rotational states are also focused by the quadrupoles. This higher rotational state background has the potential to produce systematic effects which are discussed in Sec. V B.

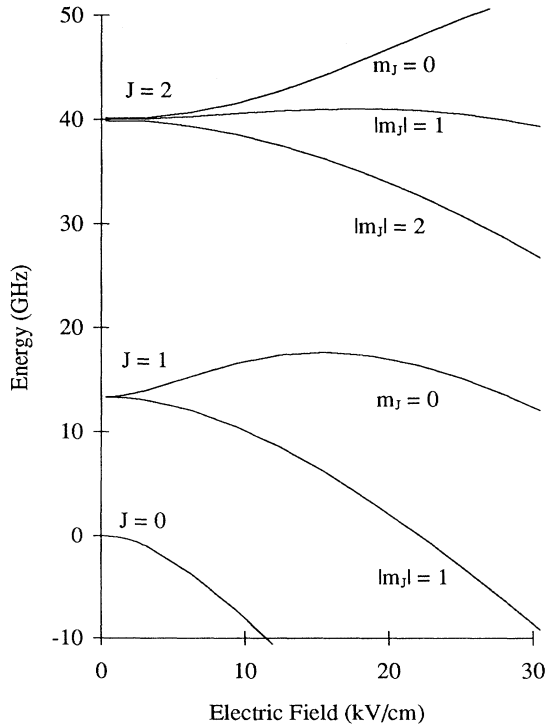

FIG. 6. Stark shifts of TlF in a high electric field for the $J=0,1,2$ rotational levels. Below 15 kV/cm the low-field seeking $|J=1, m_J=0\rangle$ states are focused by the quadrupole lens, while the $|J=1, |m_J|=1\rangle$ states are defocused.

C. Interferometer region

Two separated oscillating magnetic fields parallel to the beam direction (y direction) constitute the beam splitter and recombiner of the experiment. These are produced by a pair of coils having 20 turns on a 22 cm diameter, which are wound on a Plexiglas former outside the Pyrex beam pipe. When the coils were used to drive the 6-7 transition, their separation L was 2.051(6) m, and for the 2-3 transition we used $L=2.066(5)$ m. The resonance line shape is the characteristic Ramsey fringe pattern given in Eq. (6), in which a phase shift $\Delta\Phi$ between the atomic levels (e.g., the AC phase) can be measured as a shift of the fringes. In addition, we use the spacing of the Ramsey fringes together with the known coil separation L to determine the beam velocity.

The electric field in this region is between a pair of aluminum plates 2.45 m long, 7.6 cm high, 0.95 cm thick, and spaced by 1.99(1) cm. The focused beam travels down the center in a region approximately 1 cm in diameter, over which the average electric field is given by the infinite, parallel-plate formula V/d to better than 0.1%.

The vertical magnetic field B_x is generated by wires which run parallel to the beam, one on each side of the Pyrex beam tube. In addition, wires running along the top and bottom of the Pyrex tube can be used to null out the average horizontal magnetic field B_z. The arrangement of field plates, beam pipe, and magnetic field wires is shown in cross section in Fig. 7. The entire interferometer region is enclosed by a cylindrical magnetic shield (Ad-Mu80) to reduce the effects of the ambient laboratory field.

V. MEASUREMENTS

A. Method

The AC phase shift $\Delta\Phi_{AC}$ can be picked out by the fact that $\boldsymbol{\mu}\times\mathbf{E}$ changes sign when either E_z or B_x is reversed.

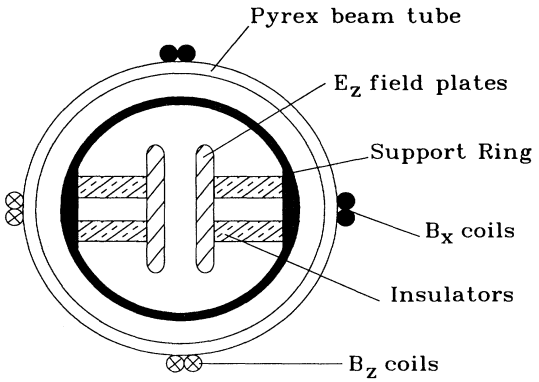

FIG. 7. Cross-sectional view of the interferometer region between the NMR coils. A pair of parallel plates produces electric field E_z. Wires on each side of the Pyrex beam tube carry equal and opposite currents to generate the vertical magnetic field B_x. Similar wires on the top and bottom generate magnetic field B_z.

TABLE II. Parameters reversed in the experiment using the 2-3 fluorine transition.

Reversal	Description	Pattern	Interval
B_x	current in B_x coil	(+−−+)	28 min
E_z	electric field	(+−−+)	80 s
P	$\pm\pi/2$ phase modulation of NMR frequency	(+−−+−++−)	150 ms
F	detuning of NMR frequency from central zero crossing	(+−−+)	4.8 s

This allows us to use a form of phase-sensitive detection in which we look for a phase shift of the Ramsey fringes in synchronism with reversals of E_z and B_x. At the central zero crossing of the Ramsey pattern, a small phase shift appears as a proportional change in the number of molecules hitting the detector. In order to convert this change in count rate to an equivalent frequency shift, we make an on-line measurement of the derivative of the resonance signal with respect to frequency at the zero crossing. Since we know that the frequency interval between zero crossings corresponds to a phase shift of π, the equivalent frequency shift can finally be converted to a measured AC phase shift.

If the magnitude of E_z changes when the electric field is "reversed," there is a Stark shift of the resonance frequency, which could be mistaken for an AC phase shift. Although such a shift does not change sign with the reversal of B_x, it is nevertheless desirable to keep this effect as small as possible. We found that commercially available high-voltage switches could cause asymmetries of tens of volts when switching a potential difference of 60 kV and that the switch lifetime was not generally as long as we would wish. We therefore used a computer-controlled, motor-driven rotary switch immersed in transformer oil (built by D. Cho), which reverses 60 kV to within 200 mV and has worked for several years without any problems. The polarity of the electric field was switched as shown in Table II at intervals of approximately 80 s in the pattern (+−−+), which was chosen to eliminate the effect of any linear drift in the beam intensity [19]. The current in the B_x coil is reversed manually by interchanging the connections at the power supply, using the same switching pattern with a period of about 28 min.

We find it useful to modulate two other quantities listed in Table II as well as the E_z and B_x reversals. In the most frequent reversal (called P in the table) the relative phase between the two rf coils is switched between $\pm\pi/2$ and the difference signal is taken. This produces the antisymmetric line shape shown in Fig. 8, on which we set the oscillator to the central zero crossing in order to be most sensitive to small phase shifts of the pattern. P reversal was performed in the sequence (+−−+−++−), which compensates for quadratic as well as linear drifts in the beam intensity [19]. We also modulated the frequency of the oscillator that drives the rf coils (F reversal), stepping it between two frequencies 1.25 Hz above and below the central zero crossing. The slope of the resonance was determined from the difference signal, while all our other measurements were averaged over the two frequencies. Details of the computer program that controlled the experiment are given in Ref. [11].

B. Previous results and systematic effect

The first set of data we acquired, utilizing the 6-7 transition, has already been published in a Letter [7]. In that work we demonstrated that the AC phase was constant for velocities in the range 217–340 m/s, that it followed the predicted electric field dependence in the 10–30 kV/cm range, and that the magnitude of the effect was as predicted at the 4% level. Limited space prevented us from discussing the two most important systematic effects which were associated with (i) the presence of a small magnetic field in the z direction; and (ii) a contribution to the resonance from molecules in $J=2$ and higher rotational states which are focused by the quadrupoles. Since these difficulties were important aspects of the first experiment and provided some of the motivation for this experiment, we now describe them.

Stray magnetic fields originating outside the magnetic shield of the interferometer region are reduced to <1 mG in the vicinity of the molecular beam, which is suitably small for our purpose. However, the coil which generates B_x is inside the shield and, since it is not perfectly aligned with respect to the electric field, it produces a stray field component B_z. In our original (6-7) experiment this stray field was approximately 40 mG when B_x

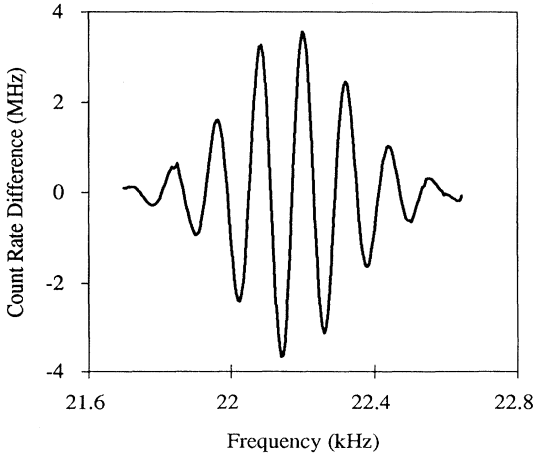

FIG. 8. Typical experimental fluorine NMR pattern obtained by switching phase between $\pm\pi/2$. We plot the difference in the detected beam intensity for the two phases.

was 0.4 G. On reversing the current in the coil, we saw a large ($\sim$80 Hz) frequency shift of the resonance due to the Zeeman effect, in addition to the much smaller AC phase shift. We are able to separate these two effects by reversing the polarity of the polarizer magnetic fields, thereby reversing the axis of quantization and selecting a state in which all the magnetic quantum numbers of the molecule are reversed relative to a fixed z axis in the laboratory. Specifically, this reverses the μ_z of the fluorine nucleus, but does not affect the induced moment μ_x, which determines $\boldsymbol{\mu}\times\mathbf{E}$. Thus we can change the sign of the Zeeman shift without changing the sign of the AC phase. In this way we were able to monitor the stray field on line and null it out using the B_z coil shown in Fig. 5. The stray field was reduced typically to $\sim$100 μG, which gave a Zeeman shift of $\sim$200 mHz. The phase shift corresponding to this frequency is comparable with the AC phase, but is easily distinguished from it because it remains unchanged when E_z is reversed.

A more insidious systematic problem is caused by the presence of higher rotational states in the beam. At first glance these would not seem to be a problem since they should only contribute to the background in the detector, not to the signal. However, in the process of going between the polarizers (where the dominant field is magnetic) and the main resonance region (dominantly electric) the ordering of the levels changes and level crossings or anticrossings necessarily occur. At these crossings, there is a possibility of Majorana transitions [20] between a focused and an unfocused state, polarizing the beam and leading to background resonances in the interferometer region. By design, there are no such transitions in the $J=1$ states, but we have not taken into account the complex level structure of all the higher rotational states. In fact, when the rf power in the polarizers is turned off, we do find a small background resonance in the vicinity of the 6-7 transition. The size varies from $\sim$1% to 10% of the 6-7 transition amplitude as the quadrupole voltage goes from 12 to 30 kV, presumably because the focusing efficiency for higher rotational states increases with higher quadrupole voltage. This resonance background is a potential source of systematic error since its amplitude changes when E_z or B_x is reversed. Fortunately it is unaffected by the rf power in the polarizers, so during the data collection in the original experiment we monitored the background resonance by switching off the rf power to the polarizers. This allowed us to distinguish the spurious background signal due to higher rotational states from the genuine AC phase shift.

C. Present experiment

The magnetic field in the polarizer (and analyzer) is used to lift the degeneracy between pairs of states that differ only in the sign of their magnetic quantum numbers. Without this field, the resonance condition for populating state 6 in the polarizer would also be the condition for driving transitions to state 5; both states would be produced and the beam would be unpolarized. However, we found that turning off the magnetic field in the polarizers reduced the size of the background resonances dramatically (to $<$0.5% of the main resonance). We were led therefore to a different experiment in which the polarizers have no magnetic field in them and we select instead state 2, a singlet which can be uniquely populated, even in zero magnetic field. The AC phase was then measured using the fluorine spin-flip transition 2-3 against a very small background of resonances from higher rotational states.

At this point some comments are needed about the eigenfunctions of the eight $m_J=\pm1$ states shown in Fig. 2. In the strong electric field $E\hat{z}$ of the main resonance region and in zero magnetic field, these states form three exactly degenerate pairs (3-4, 5-6, and 7-8) which transform into each other under time reversal, i.e., they have the same magnetic quantum numbers except for a sign. The other two are singlets (levels 1 and 2) having zero total magnetic quantum number. In the presence of a (weak) magnetic field $B\hat{z}$, the eigenstates are well approximated by those in the second column of Table III. These are the states normally discussed in the literature [11]. The representation is $|m_J,m_{\mathrm{Tl}},m_{\mathrm{F}}\rangle$, hence $|+,+,+\rangle$

TABLE III. Approximate eigenfunctions for the eight hyperfine sublevels of $J=1$, $m_J=\pm1$ in strong external electric field. The representation is $|m_J,m_{\mathrm{Tl}},m_{\mathrm{F}}\rangle$.

State	Eigenfunctions in field $B\hat{z}$	Eigenfunctions in field $B\hat{x}$
8	$\lvert-,-,-\rangle$	$\frac{1}{\sqrt{2}}\lvert+,+,+\rangle+\frac{1}{\sqrt{2}}\lvert-,-,-\rangle$
7	$\lvert+,+,+\rangle$	$\frac{1}{\sqrt{2}}\lvert+,+,+\rangle-\frac{1}{\sqrt{2}}\lvert-,-,-\rangle$
6	$\lvert+,+,-\rangle$	$\frac{1}{\sqrt{2}}\lvert+,+,-\rangle+\frac{1}{\sqrt{2}}\lvert-,-,+\rangle$
5	$\lvert-,-,+\rangle$	$\frac{1}{\sqrt{2}}\lvert+,+,-\rangle-\frac{1}{\sqrt{2}}\lvert-,-,+\rangle$
4	$\lvert-,+,-\rangle$	$\frac{1}{\sqrt{2}}\lvert+,-,+\rangle+\frac{1}{\sqrt{2}}\lvert-,+,-\rangle$
3	$\lvert+,-,+\rangle$	$\frac{1}{\sqrt{2}}\lvert+,-,+\rangle-\frac{1}{\sqrt{2}}\lvert-,+,-\rangle$
2	$\frac{1}{\sqrt{2}}\lvert+,-,-\rangle+\frac{1}{\sqrt{2}}\lvert-,+,+\rangle$	$\frac{1}{\sqrt{2}}\lvert+,-,-\rangle+\frac{1}{\sqrt{2}}\lvert-,+,+\rangle$
1	$\frac{1}{\sqrt{2}}\lvert+,-,-\rangle-\frac{1}{\sqrt{2}}\lvert-,+,+\rangle$	$\frac{1}{\sqrt{2}}\lvert+,-,-\rangle-\frac{1}{\sqrt{2}}\lvert-,+,+\rangle$

indicates $|m_J=+1\rangle|m_{\mathrm{Tl}}=+\frac{1}{2}\rangle|m_{\mathrm{F}}=+\frac{1}{2}\rangle$. However, in the present experiment, the molecules move adiabatically from the near-zero field of the polarizer into the strong transverse magnetic field B_x of the Ramsey resonance region. This causes the "time-reversed" pairs of states to be mixed and to transform adiabatically into those in the third column of the table, where one sees explicitly that transitions 6-7 and 2-3 are both fluorine nuclear spin flips. One important point concerns the 2-4 transition, which in a zero magnetic field is as strong as 2-3 and degenerate with it. Our experiment would be difficult to interpret if this were also true in the transverse field B_x, since then the resonance would involve three levels and would exhibit complicated interference effects. Fortunately this is not the case; with $B_x=1.3$ G (the field we used) the 2-4 transition amplitude is exceedingly small, as we discuss below.

First, we measured the 2-3 resonance frequency as a function of the current I_x in the B_x coil in order to test the two-level nature of the 2-3 transition. The plot of ω^2 vs I_x^2 shown in Fig. 9 verifies that the transition follows the form of Eq. (27), and from the fit we determine that $\omega_0/2\pi=22.1677(3)$ kHz. In addition, as B_x was varied, we measured the amplitude of the resonance, which is expected to remain constant in the absence of any stray field B_z. This proved to be a simple way of measuring B_z because the 2-4 transition amplitude grows very rapidly with B_z. For example, a stray B_z as small as 2 mG results in a 2-4 amplitude that is 5% of the 2-3 amplitude. Because of interference between the 2-3 and 2-4 transitions, this would appear as a comparable decrease in the height of the Ramsey pattern. The observed decrease in the resonance height was less than 2%, which reflected the fact that the misalignment of the B_x coil had been greatly reduced since our earlier experiment and now produced less than 1 mG of stray field in the z direction when $B_x\sim 1.3$ G.

Having verified the two-level character of the 2-3 transition and the absence of any significant stray B_z, we proceeded to test the velocity independence of the AC phase. We set the magnetic field B_x to a value (1.3 G) such that the resonance frequency increases to $\omega/2\pi=22.70(1)$ kHz, which corresponds to a tipping angle (Fig. 4) of 0.215(2) rad. The potential difference across the electric field plates was set to 40.0(4) kV, corresponding to an electric field of 20.1(1) kV/cm. Knowing that the spacing between the rf coils is $L=2.066(5)$ m, we use Eqs. (4) and (30) to predict a value for the AC phase of 2.47(2) mrad, shown as the solid line in Fig. 10. In the same figure, we also show the phases measured at seven different velocities ranging from 188 to 366 m/s. The weighted mean of the experimental points is 2.42(5) mrad, in excellent agreement with the theoretical expectation. We see no evidence for any deviation from the predicted velocity independence.

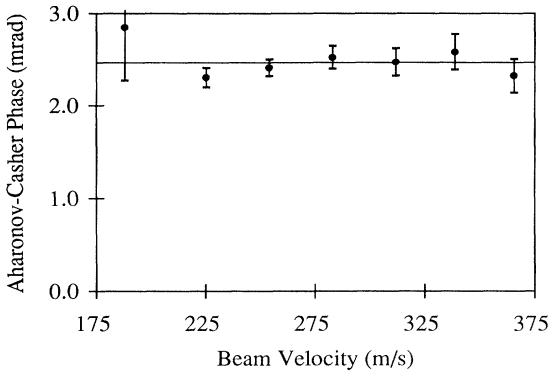

FIG. 10. Aharonov-Casher phase versus beam velocity. The solid line shows the theoretical prediction based on Eqs. (30) and (4), which has no free parameters. Points show the measured phase shifts, demonstrating the velocity independence of the phase and confirming the predicted magnitude.

Next, the velocity was fixed at 254 m/s while the electric field was varied from 5 to 20 kV/cm, as shown in Fig. 11. The theoretical prediction, shown once again by a solid line, is not quite linear in E_z due to a small Stark shift of the resonance frequencies ω_0 and ω. The experimental points show the AC phase measured at four

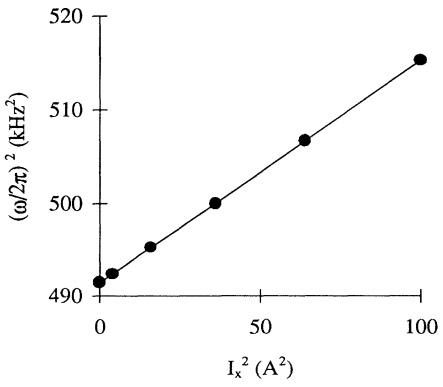

FIG. 9. Experimental plot showing the validity of Eq. (27) as a description of the 2-3 transition frequency. The straight line is a least-squares fit to the measurements.

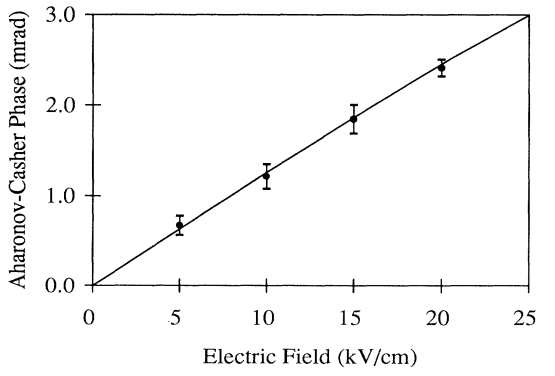

FIG. 11. Aharonov-Casher phase versus electric-field strength. The solid line shows the theoretical prediction based on Eqs. (30) and (4), which has no free parameters. Points show the measured phase shifts, demonstrating the proportionality to the electric field and confirming the predicted magnitude.

different values of the electric field, approximately 5, 10, 15, and 20 kV/cm. Again, there is no evidence of any discrepancy between theory and experiment.

The most stringent check of the theory is obtained by dividing the value of each measured phase by the corresponding predicted value. A weighted average over all the points we have measured using the 2-3 transition gives

$$\frac{\Delta\Phi_{\text{expt}}}{\Delta\Phi_{\text{theor}}}=0.98(2)\ . \tag{32}$$

VI. CONCLUSIONS

In this work we have studied the Aharonov-Casher phase, which is an analog found in neutral, spin-$\frac{1}{2}$ particles of the Aharonov-Bohm phase for charged particles. We have shown theoretically that this effect is intimately related to the Zeeman effect to all orders in v/c. We have also shown that, although it may share some of the geometric features of the Aharonov-Bohm phase, this phase can be observed without requiring that the particles encircle a line charge. Finally, we have studied the phase shifts actually exhibited by molecules moving in an electric field and we have shown that they are accurately described by the Aharonov-Casher effect at the 2% level.

ACKNOWLEDGMENTS

This work was supported in part by the National Science Foundation, the United Kingdom Engineering and Physical Sciences Research Council, the Royal Society of Edinburgh, and The Carnegie Trust for the Universities of Scotland.

[1] Y. Aharonov and A. Casher, Phys. Rev. Lett. **53**, 319 (1984); see also J. Anandan, *ibid.* **48**, 1660 (1982).

[2] Y. Aharonov and D. Bohm, Phys. Rev. **115**, 485 (1959). The relationship between the Aharonov-Bohm and Aharonov-Casher effects is described by Aharonov and Casher in [1] and in C. R. Hagen, Phys. Rev. Lett. **64**, 2347 (1990).

[3] M. V. Berry, Proc. R. Soc. London Ser. A **392**, 45 (1984); see also E. D. Commins. Am. J. Phys. **59**, 1077 (1991).

[4] Y. Aharonov, P. Pearle, and L. Vaidman, Phys. Rev. A **37**, 4052 (1988).

[5] H. Kaiser, S. A. Werner, R. Clothier, M. Arif, A. G. Klein, G. I. Opat, and A. Cimmino, in *Atomic Physics 12,* edited by J. Zorn and R. Lewis (AIP, New York, 1991), p. 247. An earlier result of the same experiment was published by A. Cimmino, G. I. Opat, A. G. Klein, H. Kaiser, S. A. Werner, M. Arif, and R. Clothier, Phys. Rev. Lett. **63**, 380 (1989).

[6] M. Kasevich and S. Chu, Phys. Rev. Lett. **67**, 181 (1991); D. W. Keith, C. R. Ekstrom, Q. A. Turchette, and D. E. Pritchard, *ibid.* **66**, 2693 (1991).

[7] K. Sangster, E. A. Hinds, S. M. Barnett, and E. Riis, Phys. Rev. Lett. **71**, 3641 (1993).

[8] R. C. Casella, Phys. Rev. Lett. **65**, 2217 (1990).

[9] N. F. Ramsey, *Molecular Beams* (Oxford University Press, Oxford, 1956).

[10] P. G. H. Sandars and E. Lipworth, Phys. Rev. Lett. **13**, 718 (1964).

[11] D. Cho, K. Sangster, and E. A. Hinds, Phys. Rev. A **44**, 2783 (1991).

[12] K. Abdullah, C. Carlberg, E. D. Commins, H. Gould, and S. B. Ross, Phys. Rev. Lett. **65**, 2347 (1990).

[13] J. J. Sakurai, *Advanced Quantum Mechanics* (Addison-Wesley, New York, 1967), p. 109.

[14] J. D. Bjorken and S. D. Drell, *Relativistic Quantum Mechanics* (McGraw-Hill, New York, 1964).

[15] T. H. Boyer, Phys. Rev. A **36**, 5083 (1987).

[16] H. Dijkerman, W. Flegel, G. Gräff, and B. Mönter, Z. Naturforsch. A **27**, 100 (1972).

[17] G. Gräff, W. Paul, and Ch. Schlier, Z. Phys. **153**, 38 (1958).

[18] P. Kusch and V. W. Hughes, in *Handbuch der Physik,* edited by S. Flügge (Springer-Verlag, Berlin, 1959), Vol. 37/1, p. 138.

[19] G. E. Harrison, M. A. Player, and P. G. H. Sandars, J. Phys. E **4**, 750 (1971).

[20] E. Majorana, Nuovo Cimento **9**, 43 (1932).